Progress in the development of the ITER baseline scenario in TCV

Progress in the development of the ITER baseline scenario in TCV

OPEN ACCESS
IOP Publishing
Plasma Physics and Controlled Fusion
Plasma Phys. Control. Fusion **66** (2024) 025016 (11pp)
https://doi.org/10.1088/1361-6587/ad1a40

Progress in the development of the ITER baseline scenario in TCV

B Labit[1,*], O Sauter[1], T Pütterich[2], F Bagnato[1], Y Camenen[3], S Coda[1], C Contré[1], R Coosemans[1], F Eriksson[4], O Février[1], E Fransson[4], A N Karpushov[1], O Krutkin[1], S Marchioni[1], A Merle[1], A Pau[1], L Piron[5,6], M Vallar[1], S Van Mulders[1], I Voitsekhovitch[6], the TCV team[8], the MST1 team[9] and the EUROfusion tokamak exploitation team[10]

[1] École Polytechnique Fédérale de Lausanne (EPFL), Swiss Plasma Center (SPC), CH-1015 Lausanne, Switzerland
[2] Max-Planck-Institut für Plasmaphysik, D-85748 Garching, Germany
[3] CNRS, Aix-Marseille University, PIIM UMR7345 Marseille, France
[4] Dept Space Earth & Environm, Chalmers University of Technology, Gothenburg, SE-41296, Sweden
[5] Dipartimento di Fisica 'G. Galilei', Università degli Studi di Padova, Padova, Italy
[6] Consorzio RFX, Corso Stati Uniti 4, 35127 Padova, Italy
[7] EURATOM/CCFE Fusion Association, Culham Science Centre, Abingdon OX14 3DB, United Kingdom

E-mail: benoit.labit@epfl.ch

Received 30 September 2023, revised 17 November 2023
Accepted for publication 3 January 2024
Published 17 January 2024

Abstract

Under the auspices of EUROfusion, the ITER baseline (IBL) scenario has been jointly investigated on AUG and TCV in the past years and this paper reports on the developments on TCV. Three ITER shapes, namely the JET, AUG and ITER IBL have been reproduced in TCV, illustrating that the higher the triangularity the larger the ELM perturbation and the more difficult it is to reach stationary states with $q_{95} < 3.6$. It is found that the performance of TCV IBL is mainly limited by (neoclassical) tearing modes, in particular 2/1 modes which are triggered after a large ELM. It is demonstrated that the shorter the ELM period the larger β_N at the NTM onset. We show that these modes can be avoided with central X3 EC heating at relatively high q_{95} and moderate β_N. However, the lack of significant ECH at the high central densities obtained in TCV IBL scenario limits the duration of low q_{95} cases to about four confinement times. During this time, density usually keeps peaking until (neoclassical) tearing modes are triggered. Nevertheless, the TCV IBL database covers the ITER target values ($H_{98y2} \sim 1$, $\beta_N \sim 1.8$ at $q_{95} \sim 3$) and a slightly better confinement than requested for ITER is

[8] See author list of 'H Reimerdes *et al* 2022 *Nucl. Fusion* **62** 042018'.
[9] See author list of 'B Labit *et al* 2019 *Nucl. Fusion* **59** 086020'.
[10] See the author list of 'Progress on an exhaust solution for a reactor using EUROfusion multimachines capabilities' by E Joffrin *et al* to be published in Nuclear Fusion Special Issue: Overview and Summary Papers from the 29th Fusion Energy Conference (London, UK, 16–21 October 2023).

* Author to whom any correspondence should be addressed.

reported. Integrated modelling results show that ITG modes are the dominant instabilities, and show that, in TCV, fuelling also plays a role to sustain peaked density profiles. The role of profiles, sawteeth and ELMs regarding MHD stability are also discussed.

Keywords: ITER baseline scenario, neoclassical tearing modes, pedestals

1. Introduction

The ITER baseline (IBL) scenario is the inductive 'standard' ELMy H-mode scenario aiming for $Q = 10$ performance in ITER [1] with plasma operation at full plasma current (15 MA) and full toroidal magnetic field (5.3 T). The IBL scenario is investigated in various tokamaks [2–6] and the current paper focuses on the developments of the IBL in TCV based on the know-how obtained on AUG within cross-machine experiments conducted by EUROfusion. The IBL scenario can be defined with low q_{95}, aiming for $q_{95} = 3$, high β_N ($\beta_N = 1.8$), high elongation, aiming for $\kappa = 1.8$, high Greenwald fraction ($f_G = 0.8$) and a large positive triangularity $\delta = 0.5$. Indeed, the IBL scenario is based on the confinement improvement of ELMy H-modes with increasing positive triangularity, thanks to an increase of the average top pedestal pressure through an improved edge stability. Note that the ITER triangularity is very high and is at the top of the highly sensitive dependence of pedestal top pressure versus triangularity as shown by EPED-CH simulations in figure 10 of [7]. It is shown that a change of δ from 0.3 to 0.5 can almost double the predicted pedestal pressure. One has to remember also that an important parameter for transport, the pedestal collisionality cannot be reduced to ITER values in current machines, in particular at large plasma densities and it is not usually used when comparing different IBL scenarios.

The installation of a neutral beam injector (NBI) on TCV [8], together with the well known shaping capabilities of this device allowed the investigation of ELMy H-modes at ITER relevant β_N and shapes. The initial developments of the scenario on TCV have been reported in [9].

The paper is organised as follow: in section 2, the strategy used to develop the scenario and the shape adjustements are explained. The role of neoclassical tearing modes (NTMs) in particular on the disruptivity of the scenario is discussed in section 3. We will then focus on the developments of safe termination strategies, guided by predictive optimization simulations (section 4). Section 5 will summarise the performances of the IBL database in TCV. Finally, we shall discuss heat and particle integrated modelling, using ASTRA-GLF23 and GENE in section 6 before concluding (section 7).

2. Scenario and shape development

Initially, a similar strategy as the one used on AUG [10] was tested on TCV. It consisted in entering in H-mode once the final plasma shape was already established and the flat-top plasma current reached (aiming at $q_{95} \sim 3$). Nevertheless, this approach led systematically to early disruption either because of an ELM free phase with uncontrolled density increasing up to the density limit or because of a very large ELM inducing a vertical displacement event (VDE). Consequently, the strategy has been revised and a typical IBL scenario in TCV is illustrated in figure 1. The pulse can be divided into the following sequences:

- Phase 1: The H-mode was initiated during the plasma current ramp ($I_p \sim$ 170 kA, $q_{95} > 4$) with reduced shaping ($\kappa \sim 1.5$, $\delta \sim 0.35$) by a NBI power ramp up to 1.1 MW. Stationary conditions were obtained with regular ELMs, seen on the D_α trace (figure 1(e)), which controlled the plasma density (figure 1(c)).
- Phase 2: At $t = 1.1$ s, the flattop plasma current value was reached ($I_p \sim$ 250 kA, $q_{95} \sim$3.6) and the plasma shaping was completed ($\kappa \sim 1.7$, $\delta \sim 0.45$). As a consequence, the ELM frequency decreased and the ELMs became larger. The good performances for the IBL scenario ($\beta_N >$1.8, $H_{98y2} \simeq$ 1) were achieved during this phase which last on average for about 5 energy confinement times (see section 5).
- Phase 3: At $t \simeq$1.2 s, a 2/1 NTM was triggered after an ELM and consequently, plasma performance degraded significantly ($\beta_N \sim 1.2$). Eventually, the mode locked at 1.38 s. As it will be seen in the next section, NTMs were the main limiting factor for good confinement of IBL scenarios on TCV.
- Phase 4: As it will be discussed in section 4, the exit of the H-mode is a delicate phase and usually, as in the case here, the plasma disrupted couple of ms after the NBI was stopped.

Using this strategy, the shaping capabilities of TCV have been used to develop similar IBL shapes than the ones used in AUG and JET which differ from the exact ITER shape. In particular the plasma triangularity on both devices is reduced ($\delta_{\rm AUG} \simeq 0.25$, $\delta_{\rm JET} \simeq 0.35$) compared to the expected value in ITER. Figure 2 summarizes the results with spider plots comparing ITER main parameters with those achieved on TCV, AUG and JET. It has to be noted that usually the value of q_{95} is not matched on TCV because of the extreme level of disruptions for this scenario.

3. Role of MHD in limiting the performance of the IBL scenario

3.1. Onset of neoclassical tearing modes triggered by ELMS

NTMs were very often observed in these TCV IBL scenarios, usually 3/2 or 2/1 modes which can lock and unlock depending on the plasma profiles evolution. The poloidal and toroidal mode numbers have been identified with phase analysis of different arrays of magnetic probes [11]. They could be born as tearing mode but in most of the cases they were triggered by

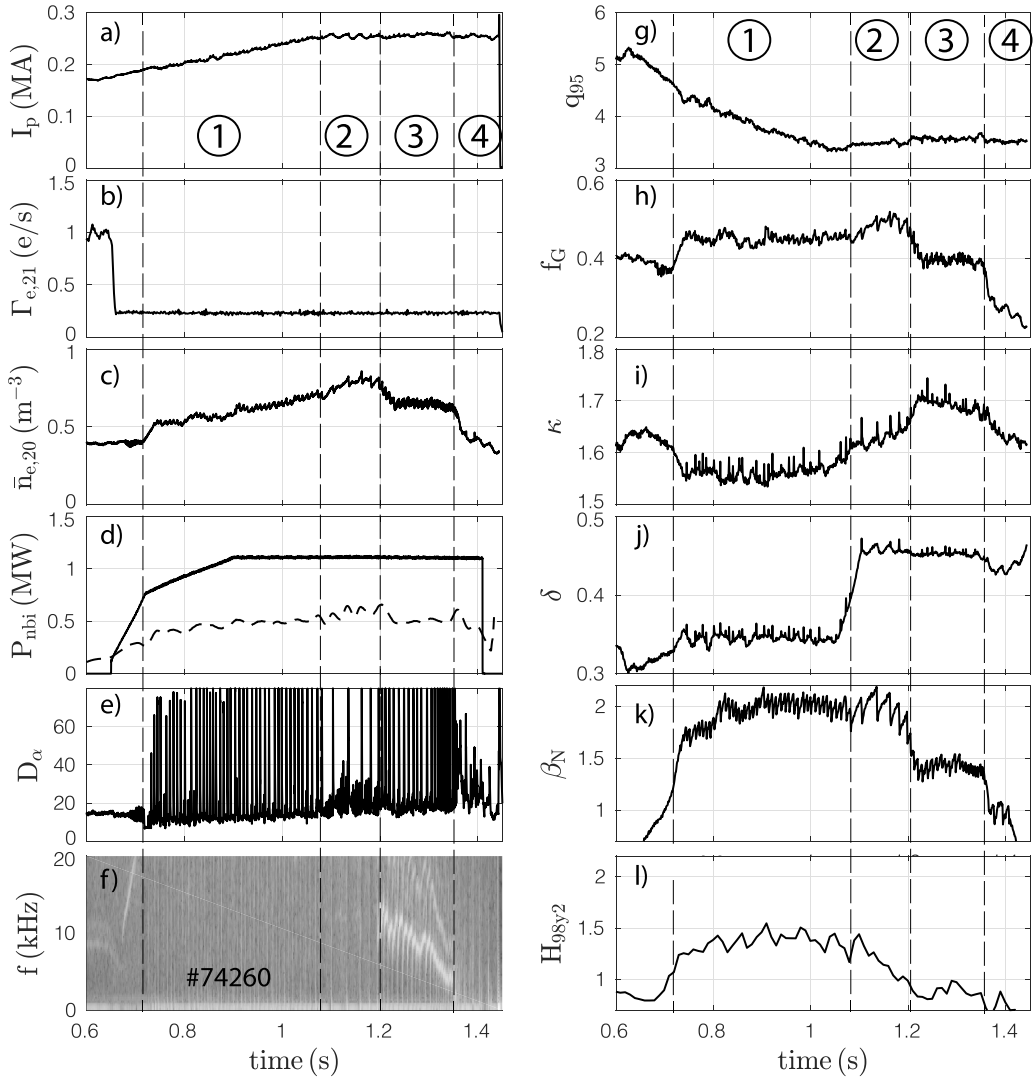

Figure 1. Main time traces (#74260) to illustrate the strategy used to develop the IBL scenario at TCV. The H-mode period can be divided into four phases. (a) plasma current, (b) deuterium flow, (c) line averaged density, (d) NB injected power (solid) and radiated power (dashed), (e) D_α signal, (f) magnetics spectrogram, (g) safety factor, (h) Greenwald fraction, (i) elongation, (j) averaged triangularity, (k) normalised beta, (l) confinement factor.

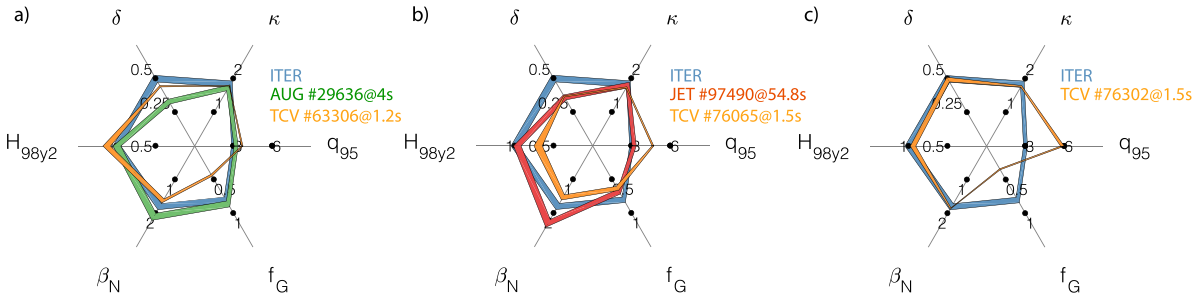

Figure 2. Spider plots for the ITER (blue) and TCV (yellow) and comparison with (a) AUG (green) and (b) JET (red), (c) TCV case matching ITER shape.

the large ELM crashes, which have $\Delta W/W_{\mathrm{mhd}} \sim 20\%$ where ΔW is the averaged lost energy during ELMs and W_{mhd} is the plasma stored energy. Indeed, tearing modes are more unstable with a broad current density profile and therefore can more easily be made unstable by external perturbations. In TCV IBL, the modification of the pressure profile due to ELMs can

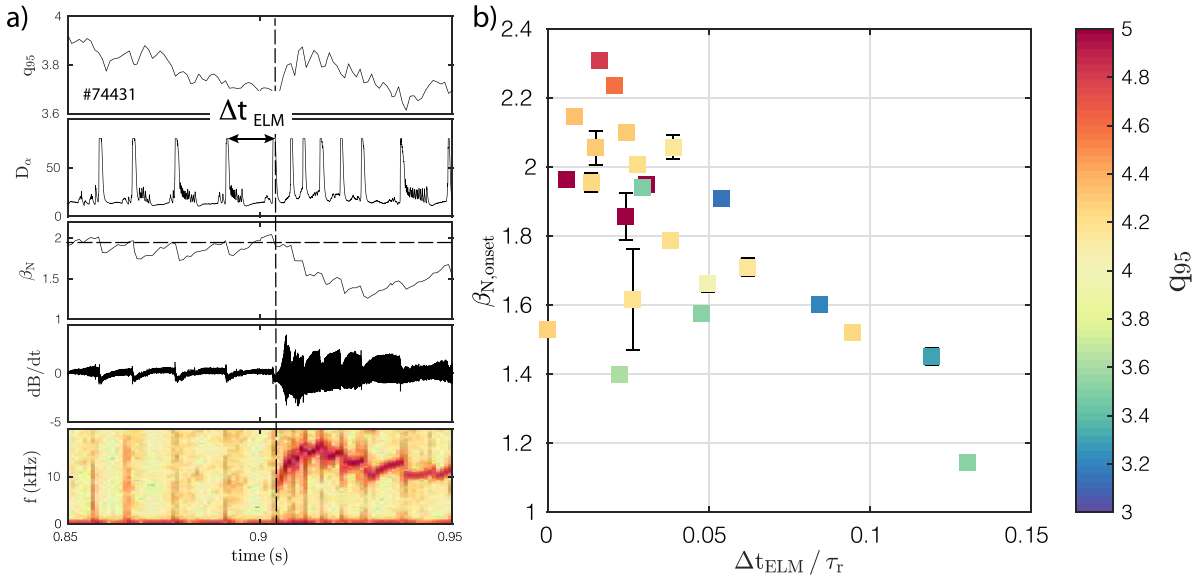

Figure 3. Normalised beta β_N as a function of normalised ELM period Δt_{ELM}. Data are colour coded with q_{95}.

be seen up to mid-radius well beyond the location of the $q = 2$ surface ($\rho_\psi(q = 2) \simeq 0.7$). In addition, the density peaking is significant, especially when comparing with AUG cases. This led to flat and broad T_e profiles, often the loss of sawteeth ($q > 1$), and therefore broad current density profiles.

We have further investigated the conditions when NTMs were triggered by ELMs, making an analogy between ELMs and sawteeth. Indeed, like large sawteeth, large ELMs can seed islands or modify the local magnetic shear. In [12], a clear relationship between the sawtooth period, normalised to a resistive time, and the β_N value at the NTM onset was established for a multi-machine database. As illustrated in figure 3(a), for a subset of the IBL database for which NTMs were clearly triggered by an ELM, the β_N value at the NTM onset together with the elapsed time between the ELM which triggered the NTM and the previous one (Δt_{ELM}) was recorded. The results are reported in figure 3(b) where $\beta_{N,\mathrm{onset}}$ is ploted as a function of the normalised 'ELM period' Δt_{ELM} and colour coded with q_{95} values. A clear linear trend is observed indicating that the shorter is the 'ELM period', the larger is the achievable β_N before the NTM is triggered. It can be noted also that the largest values for β_N are obtained at large q_{95}. For potential cross-machine comparison, the 'ELM period' has been normalised to a resistive time defined as $\tau_r = \frac{\mu_0 a^2}{1.22\eta_{\mathrm{neo}}(\rho=0.4)}$, where the neoclassical resistivity, evaluated at $\rho_\psi = 0.4$, is proposed as a volume-averaged value.

3.2. Cause of disruption for the IBL scenario

For most of the cases, plasmas disrupted when one tried to reach $q_{95} \sim 3$ at full shaping and therefore it seemed necessary to look at the causes of these disruptions. For that purpose, we analysed 113 shots with a machine agnostic object-oriented framework, *DEFUSE* [13], a major upgrade of the previous code *DIS_tool* [14]. This hybrid framework leveraged physics-based scalings, statistical and machine learning approaches to efficiently automate extremely time-consuming tasks, namely the detection and annotation of plasma state sequences, transient events, disruption precursors and consequences. Figure 4 shows the statistics for the main disruption patterns affecting the TCV IBL scenario. It is found that about 70% of the disruptions were due to issues with vertical stability control. Indeed, for the majority of cases (*Vertical Displacement with rotating mode* in figure 4), large ELMs are exciting $n = 0$ modes and once a rotating NTM ($n = 1$) was triggered, both modes coupled and led to VDEs. Regarding the physics mechanisms,

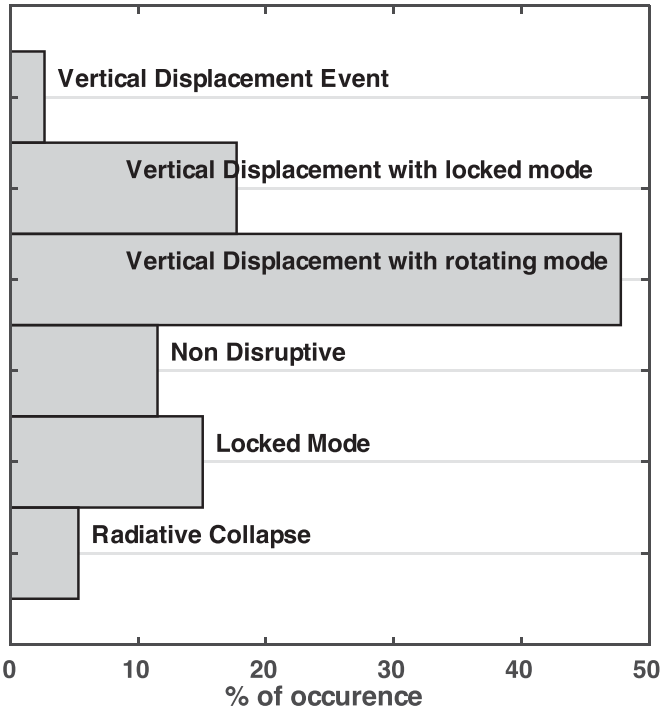

Figure 4. Probability distribution of the various causes of the disruptions for the IBL scenario on TCV.

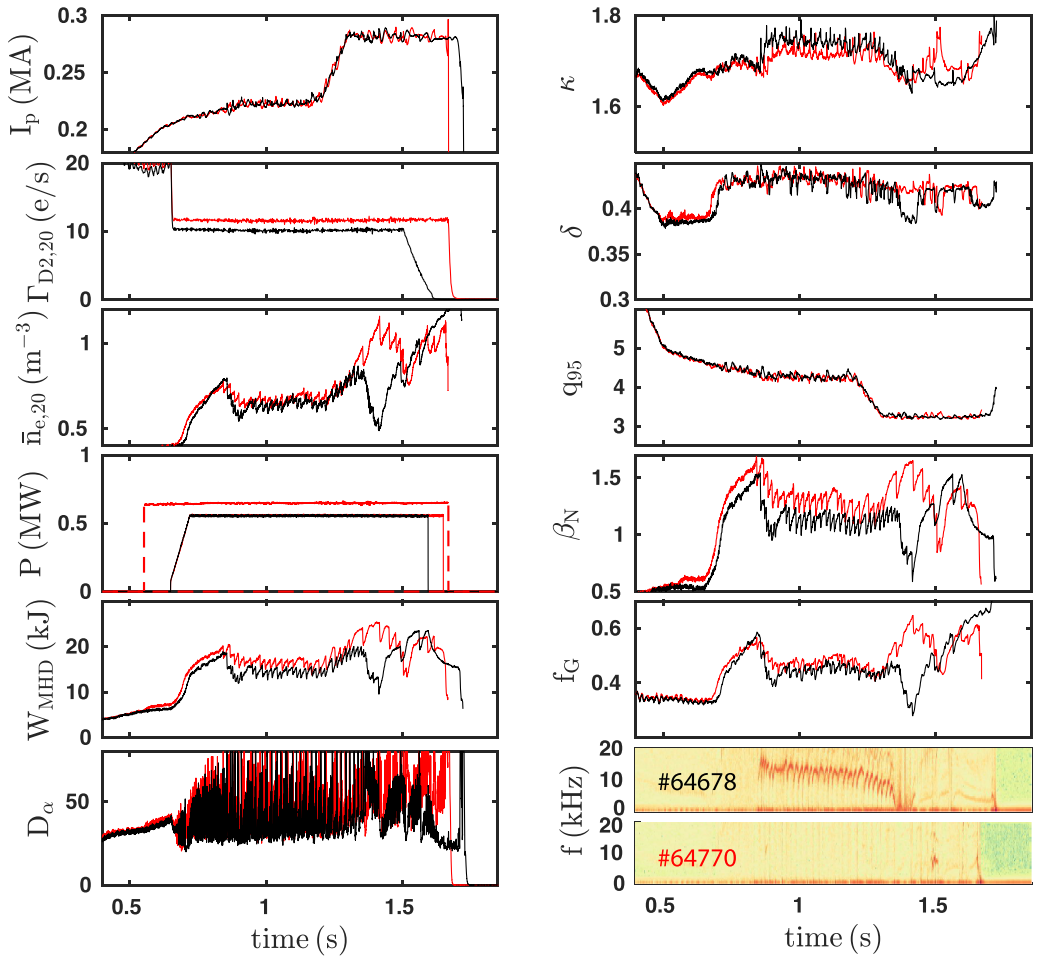

Figure 5. Time traces of two TCV IBL discharges with (#64770, red) and without (#64678, black) X3 central EC heating. A 2/1 mode is triggered at 0.86 s in #64678 at the first large ELM, while only a small n even mode at ∼40 kHz appears in #64770.

each ELM event causes a *small* vertical displacement, which is essentially a magnetic perturbation with $n = 0$ component, due to a drop in poloidal beta. There are also several studies on the experimental demonstration of ELM pacing through vertical kicks, which is based on the same principle.

3.3. Prevention of neoclassical tearing modes with ECR heating

We have tested the role of input power and electron heating in a series of otherwise similar discharges with a first phase at high $q_{95} \sim 4.2$ $(0.8 < t < 1.2$ s) and a second phase with $q_{95} \sim 3.2$ $(1.3 < t < 1.7$ s). In the first discharge, #64678, shown in black in figure 5, a 2/1 mode appeared in the first phase and degraded the confinement. On the other hand, adding ECR X3 heating, as in shot #64770 shown in red, avoided this mode onset, although a similar first large ELM occurred, but only an even n mode at ∼40 kHz was triggered (small 3/2) which disappeared when I_p was increased at 1.2 s. The 2/1 mode could eventually lock (as for instance at 1.35 s in #64678) and usually led to significant confinement degradation followed by an abrupt H-L back transition and most likely a disruption. The mode locking could also lead to a sufficient drop in β and kinetic profiles to stabilize the NTM, after which the discharge recovered quickly. So it should underlined that the 2/1 mode locking in itself did not trigger a disruption.

One has to remember that the energy confinement time in TCV is $\tau_E \sim$ 20–30 ms, therefore TCV IBL were sustained for $\sim 5\tau_E$ for q_{95} ∼3.2 and $> 10\tau_E$ for q_{95} >3.6. As seen for shot #64770 around 1.4 s, the low q_{95} phase had large β_N for a couple of ELM periods, until a mode was triggered. Since the ELM period is 40–60 ms, about 2–3 τ_E, this was the main limitation for the high performance duration. Nevertheless, this duration is long when compared to the typical current redistribution time on TCV (∼100 ms). This might explain the large perturbation caused by the ELM crash and is consistent with the occurrence of 2/1 modes after a few ELMs, as observed in [6].

Using the scenario of #64678, the ability of ECRH to prevent the NTM formation has been further evaluated with a scan in the NB injected power, while the injected ECRH X3 power remained constant at 0.8 MW. We focused on the early phase with low shaping and reduced plasma current so all quantities have been averaged over the period $0.9 < t < 1.1$ s ($q_{95} = 4.3$,

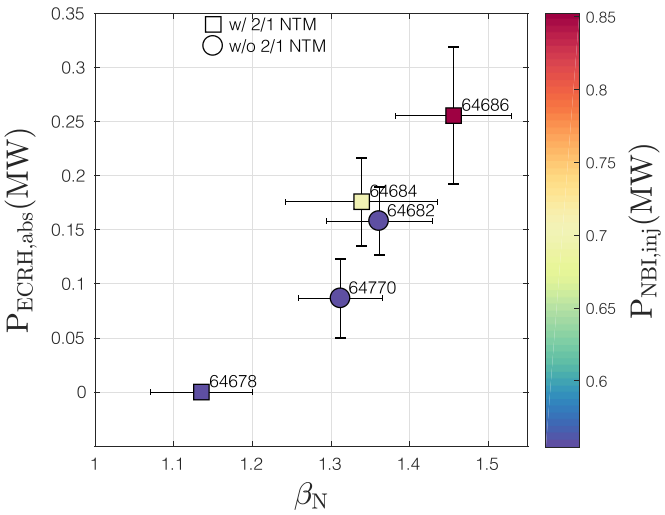

Figure 6. Absorbed ECRH power as a function of the achieved β_N for otherwise similar conditions, except the NB injected power. Square symbols indicate the presence of a 2/1 NTM while the absence of modes is shown with circle symbols. All quantities are averaged between 0.9 and 1.1 s.

$\delta = 0.43$, $\kappa = 1.72$). The results are summarised in figure 6 where the absorbed ECRH power is plotted as a function of the time averaged β_N. It was observed that at larger injected NBI power ($P_{\mathrm{NBI,inj}} > 0.6$ MW) hence larger β_N, a 2/1 NTM developed even if the coupled ECRH power was increased with respect to #64770 (#64684, #64686). The absorbed EC power was found to increase with β_N because at larger β_N, the electron temperature profiles were more peaked and the EC coupling was improved. In future experiments, one has to see if adding another 0.8 MW from the second X3 gyrotron will be enough to stabilise the NTM for $\beta_N > 1.65$ which is the value at the NTM onset in #64684. While shots #64684 and #64682 have almost the same β_N and the same ECRH absorbed power, the former developed a NTM while the latter did not. Actually, one difference between both shots is the density peaking which is slightly larger for #64684 compared to #64682. The increase in density peaking, probably due to a larger beam fuelling, flattened the temperature profile thus the current profile was broaden and consequently more prone to MHD instabilities. From these discharges and others not discussed here, it can be confirmed that it was the combination of large β_N, peaked density profiles, high elongation and large ELMs which forced the triggering of 2/1 modes after a few ELM crashes and reduced the performance of the IBL in TCV.

For the early phase of these shots, it has to be noted that only about 10%–15% of the NBI power goes to the electrons and about 25% to the ions. The rest of the power was lost either from first orbits or from CX reactions. In order to be conservative, the CX losses were not removed in the computation of the H_{98y2} factor. This led typically to a 10%–20% underestimation. Finally, in the later phase of these shots when the plasma current was increased to reach $q_{95} \sim 3$, β_N remained large or even increased and it was attributed to an increase in density together with a better NBI coupling (reduced first orbit and CX losses).

4. Safe plasma termination for IBL scenario

As it has been seen in the previous section, the disruptivity on the IBL scenario is very large. Therefore it is crucial to optimize the strategy for the plasma ramp-down and the H-L back transition. Integrated modelling of AUG discharges including the ramp-down phase has been performed using the RAPTOR code [15], and then an optimization procedure for the termination phase has been conducted, also described in [16]. The main ingredients for a safe yet rapid termination are a decrease of plasma current together with a decrease of elongation, while controlling the heat sources during the whole termination. The goal being to trigger a H-L transition at about 1/3 of the ramp-down, the elongation should not decrease too fast, in order to avoid too low q_{95} values, and the H-L transition should not occur too late to avoid a too large Greenwald fraction. These key ingredients allow a control of the time evolution of the internal inductance ℓ_i, the elongation κ and the power balance. The simulation results were then used to design the termination segment for IBL scenarios in TCV. A test case (#76775) is shown in figure 7, where a high plasma current case (170 kA) safely ramped down to 70 kA, with a controlled H-L transition about 1/3 into the NB ramp-down and an elongation decreasing while decreasing I_p. In particular, the late H-L back transition forced a slow increase of the internal inductance and a stable plasma, even though the shape was oscillating between limited and diverted as seen on the time evolution of κ and δ. We repeated the shot without the reduction in elongation (#76776) and it disrupted with a VDE right after the H-L transition, consistent with an increase of the $n = 0$ growth rate with elongation. Nevertheless, the internal inductance evolved similarly in both shots, and it was rather the critical ℓ_i for VDE which was reduced for the same plasma current, in this case. Both ramp-down phases have been simulated and optimised with the RAPTOR code, suggesting, for instance, that delaying the NBI ramp-down could lead to a safer plasma termination [17]. These studies have also been used to develop the real-time termination algorithm used in JET baseline scenarios [18].

5. Performance of the ITER baseline scenario on TCV

The main figures of merit are the H_{98y2} scaling factor and normalized pressure β_N. The TCV IBL results are reported in figure 8 including the pedestal top values for electron temperature and density, following the definitions in [19] (figure 8(b)). As discussed in [3], AUG focussed on two IBL scenarios with $q_{95} \sim 3$ and $q_{95} \sim 3.6$ indicated with the red dashed lines in figure 8(a) and TCV results are also compared to both pairs of values. The black dashed lines represent constant H_{98y2}/β_N values with similar performance properties if $q_{95} \propto \beta_N$ (constant $H_{98y2}\beta_N/q_{95}^2$). They also reflect the observed confinement improvement with β_N not included in H_{98y2}. It is interesting to note that the TCV data points align relatively well with slightly better confinement properties than the required ITER target, consistent with previous carbon wall

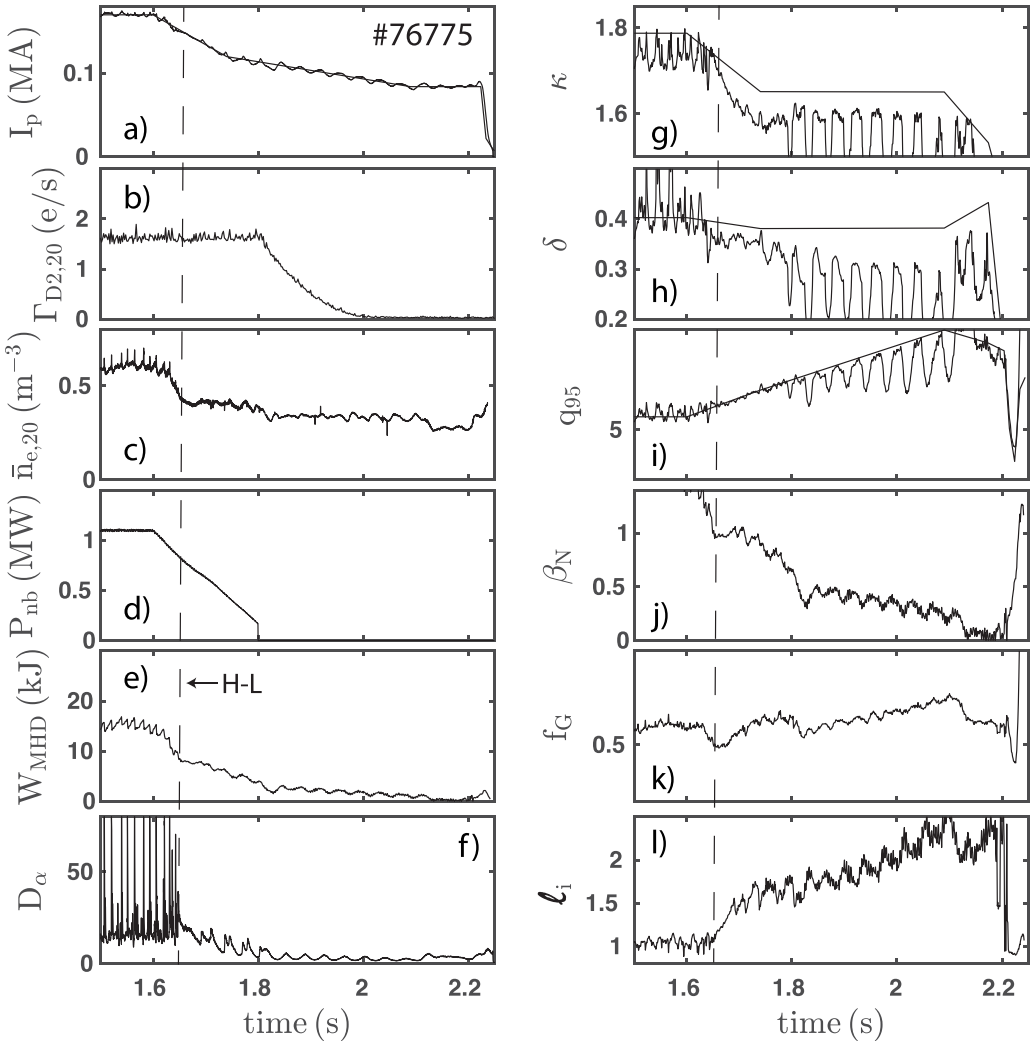

Figure 7. Time traces of #76775 for which the ramp-down was improved following a strategy derived from RAPTOR simulations. (a) plasma current, (b) deuterium flow, (c) line averaged density, (d) injected NB power, (e) stored energy, (f) D_α, (g) elongation, (h) averaged triangularity, (i) safety factor, (j) normalised beta, (k) Greenwald fraction, (l) internal inductance.

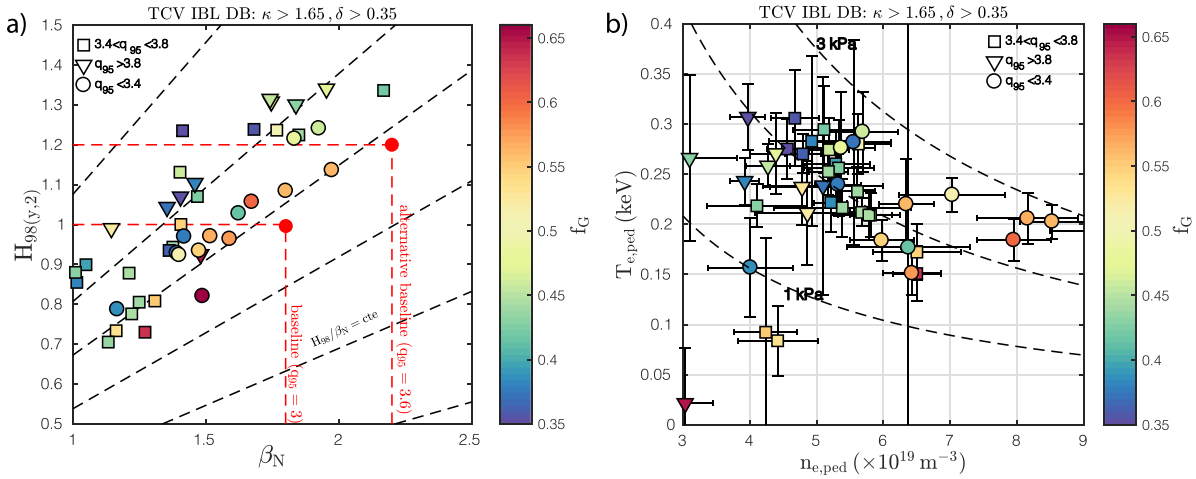

Figure 8. TCV IBL database with $\kappa > 1.65$ and $\delta > 0.35$. (a) H_{98} vs β_N; (b) Pedestal top electron temperature vs pedestal top electron density. Both plots are colour coded with the Greenwald fraction f_G.

studies. Actually, AUG IBL with carbon wall had better confinement properties and spanned the region at and above the ITER point ($\beta_N = 1.8$; $H_{98y2} = 1.$), and its alternative with similar performance ($\beta_N = 2.2$;$H_{98y2} = 1.2$) [2, 4].

In figure 8(b), it can be seen that the TCV IBL database spans about a factor of two in pedestal pressure, although most points are at about 2 kPa. The higher density cases tend to follow the lower confinement dashed line, combined with lower q_{95}, while the higher confinement points tend to have larger q_{95} and lower f_G. In addition, the observed confinement improvement with β_N at large f_G is consistent with an increase of $n_{e,\mathrm{ped}}$ at constant $T_{e,\mathrm{ped}}$.

As reported in [2], a degradation of confinement at higher Greenwald fraction is expected, which is usually alleviated by increasing the edge triangularity. The TCV IBL data is consistent with this trend showing a maximum H_{98y2} factor around 1.5 for $f_G \sim 0.4$ and about 1 for $f_G \sim 0.6$. However, the points near this trend are not at the highest δ values, and have rather smaller elongation. This is consistent with the experimental strategy used in TCV: ELMy H-modes are much more reliable at lower elongation and less perturbed by Type-I ELMs. It has to be noted also that the density limit in TCV is usually below $f_G \sim 1$. In addition, higher elongation leads to naturally lower internal inductance ℓ_i and broader current density profiles [20], which can explain a lower density limit or higher sensitivity to density peaking for the triggering of 2/1 modes in particular. This is consistent with the important role of the slow time evolution of the current density profile shown in DIII-D IBL [6] and consistent with the role of both the global q profile and the increased magnetic shear near q = 2 on tearing mode stability observed on TCV and included in a varying tearing parameter Δ' within the modified Rutherford equation [21].

6. Transport modelling

The capability of a quasi-linear drift mode based transport model to predict the thermal and particle transport in TCV ITER baseline scenario is examined for #64770 ($q_{95} \sim 3.2$). The evolution of electron (T_e) and ion (T_i) temperatures and main ion (n_D) as well as the poloidal field diffusion equation are simulated in the whole plasma region ($\rho_\psi = 0$–1) with ASTRA code starting in the ohmic phase ($t = 0.5$ s) and finishing at the end of the high plasma current flat-top. The NBI simulations are performed self-consistently with plasma evolution taking into account the shine-through, CX and orbit losses, while the TORAY-GA code is used for the ECRH/ECCD modelling performed with the measured plasma profiles. The transport model applied here combines the GLF23 computed transport coefficients in the core region ($0 < \rho_\psi < 0.85$) with ad-hoc edge transport coefficients and NCLASS used for the thermal and particle transport as well as current conductivity and bootstrap current. The GLF23 model is used here as a numerically fast approximation to TGLF which allows to simulate the entire scenario in a computationally reasonable time while providing important information on the microturbulence stability and the effects potentially stabilising anomalous transport. The impact of observed sawtooth oscillations is taken into account by increasing the transport coefficients within mixing radius simulated self-consistently with the q-profile evolution assuming the Kadomtsev reconnection model. In addition, the feedback control of the volume averaged density via the neutral influx is applied. In the absence of T_i measurements the diamagnetic energy W_{dia} extracted from the diamagnetic flux measurements and consistent with the equilibrium reconstruction has been used for comparison with W_{dia} obtained in transport modelling.

The temperature and density evolution in #64770 gives an indication of strong electron temperature stiffness—both simulated and experimental electron temperature weakly evolve during the discharge in spite of the strong density increase and reduced auxiliary electron heating from 0.25 MW at 1.2 s to 0.16 MW at 1.4 s—mainly due to a reduced ECRH absorption at high density.

In addition, this discharge is characterised by a strong density peaking which is reasonably predicted up to the central density values of $(10\text{–}12) \times 10^{19}\mathrm{m}^{-3}$ and underpredicted at higher n_e (#64770, 1.4 s). It should be mentioned that the drift modes are stable within $\rho_\psi = 0.2$ in performed simulations and the transport in the central region is determined by NCLASS enhanced by the sawteeth mixing.

Those self-consistent transport simulations show that ITG is the dominant instability in a broad plasma region ($0.3 < \rho_\psi < 0.8$) during the quasi-stationary phases achieved at the plasma current flat-top. These results are consistent with the microturbulence stability analysis performed with local linear runs of the GENE code for the same discharge and compared to #64678 featuring a NTM. Temperature and density profiles together with frequencies ω and growth rates γ, both normalised to the ion sound speed c_s are plotted in figure 9. These simulations included collisions, electromagnetic effects, two kinetic species and $T_i = T_e$ was used. The analysis was done at two radial positions: in the plasma core ($\rho_\psi = 0.5$) and at the pedestal top ($\rho_\psi = 0.9$). For long wavelenghts ($k_y\rho_s < 1$), positive frequencies indicate that ITG sis the dominant instability, and this is the case for both shots and both locations. In more details:

- For both shots at $t = 1.1$ s and $\rho_\psi = 0.9$, the normalised grandients are very similar and so the growth rates are almost identical.
- For #64678 at low shaping/large q_{95} ($t = 1.1$ s), even if the temperature profile is flattened by the NTM at $\rho_\psi \sim 0.65$, the central temperature is close to the value for #64770 without the NTM ($T_e(0) \sim 0.8$ keV). This indicates that R/L_{T_e} is larger at $\rho_\psi = 0.5$ in #64678 and so both the growth rate and the frequency of the ITG mode is larger for the shot featuring the NTM.
- During the high performance phase of #64770 ($t = 1.4$ s), normalised gradient lenghts for both density and temperature are larger compared to the phase at low shaping/large q_{95} ($t = 1.1$ s). In consequence, the normalized ITG mode growth rate is almost doubled from $t = 1.1$ s to $t = 1.4$ s at $\rho_\psi = 0.5$.

shot	time (s)	ρ_ψ	R/L_n	R/L_{Te}
64678	1.1	0.5	2.4	6.9
64770	1.1	0.5	2.5	4.1
64770	1.4	0.5	3.3	5.3
64770	1.1	0.9	1.5	7.4
64678	1.1	0.9	1.5	5.3

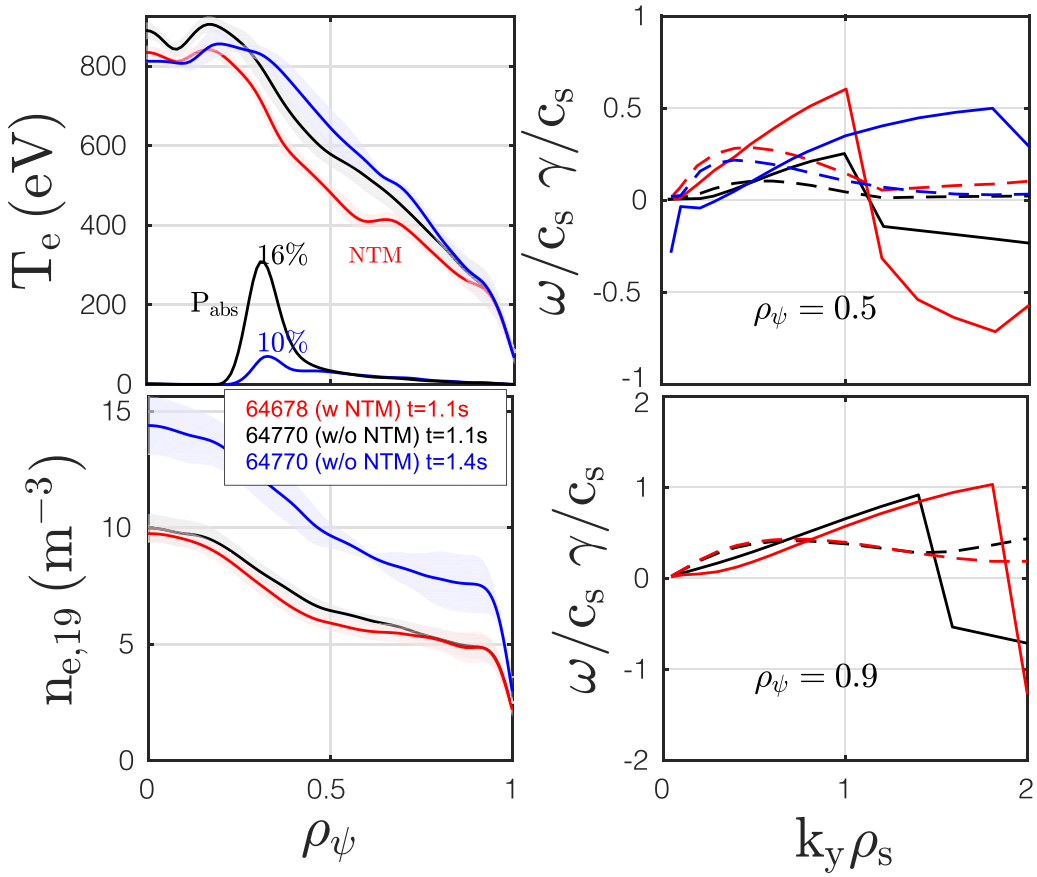

Figure 9. Linear gyrokinetic analysis Microturbulence growth rates (dashed) and frequencies (solid) at mid-radius and at pedestal top in TCV #64770 using GENE. Positive frequencies correspond to ITG modes.

7. Conclusions

The ITER baseline scenarios have been successfully developed in TCV and analysed. The strategy consisted in entering in H-mode at large q_{95} and reduced shaping in order to get regular ELMs not too large. Notably, this could be performed while both q_{95} and the plasma shape were evolving. The final shape and plasma current were reached in a second phase and good performance was obtained for durations of about five energy confinement times. From there, the AUG IBL shape, the JET IBL shape and the exact ITER shape were matched but at reduced plasma current (and Greenwald fraction).

Indeed, the level of disruptions for the IBL scenario is very height and it has been found that about 50% of the disruptions were caused by a vertical displacement in presence of a rotating mode, which was triggered by large ELMs. It was shown that broad current density profile, induced by density peaking, as well as elongation, high β_N and low q_{95} combined to force more unstable plasma to classical and NTMs. These modes could be avoided at medium β_N and/or high q_{95} with X3 EC heating, and also at lower elongation. We have used the benefit of controlled elongation and power source during AUG IBL termination phases (in feedforward). Initial tests for a safe ramp-down scenario, inspired by off-line optimization from RAPTOR simulations have been performed but

further optimisation remains possible. The TCV IBL database covered the ITER target values (H_{98y2} ∼1, β_N ∼1.8 at q_{95} ∼3 and H_{98y2} ∼1.2, β_N ∼2.2 at q_{95} ∼3.6) and a slightly better confinement was reported and was consistent with previous findings with machines featuring carbon walls. Integrated modelling using ASTRA-GLF23 quasi-linear drift mode based transport model predicted the observed heat and particle transport, with ITG dominant regime across most of the radial domain. In particular, it was able to reproduce the mainly turbulent-driven significant density peaking observed in TCV IBL discharges.

The development of the IBL scenario on TCV will continue in the next experimental campaigns with the use of the second X3 gyrotron and the second NBI together with impurity seeding for detachment studies. The results obtained on both AUG and TCV will continue to mutually feed the developments on both devices.

Data availability statement

The data that support the findings of this study are available upon reasonable request from the authors.

Acknowledgments

This work has been carried out within the framework of the EUROfusion Consortium, partially funded by the European Union via the Euratom Research and Training Programme (Grant Agreement No. 101052200 - EUROfusion). The Swiss contribution to this work has been funded by the Swiss State Secretariat for Education, Research and Innovation (SERI). Views and opinions expressed are however those of the author(s) only and do not necessarily reflect those of the European Union, the European Commission or SERI. Neither the European Union nor the European Commission nor SERI can be held responsible for them. This work was supported in part by the Swiss National Science Foundation.

ORCID iDs

B Labit https://orcid.org/0000-0002-0751-8182
O Sauter https://orcid.org/0000-0002-0099-6675
T Pütterich https://orcid.org/0000-0002-8487-4973
S Coda https://orcid.org/0000-0002-8010-4971
R Coosemans https://orcid.org/0000-0001-8110-3156
F Eriksson https://orcid.org/0000-0002-2740-7738
O Février https://orcid.org/0000-0002-9290-7413
E Fransson https://orcid.org/0000-0002-8747-3470
O Krutkin https://orcid.org/0000-0002-9124-2659
A Merle https://orcid.org/0000-0003-1831-5644
A Pau https://orcid.org/0000-0002-7122-3346
L Piron https://orcid.org/0000-0002-7928-4661
M Vallar https://orcid.org/0000-0002-1792-6702
S Van Mulders https://orcid.org/0000-0003-3184-3361

References

[1] Shimada M *et al* 2007 Chapter 1: overview and summary *Nucl. Fusion* **47** S1
[2] Sips A C C *et al* (JET Contributors, The ASDEX Upgrade Team, The DIII-D Team, The C-Mod Team, The JT-60U Team, members and ITPA-IOS TG Experts) 2018 Assessment of the baseline scenario at $q_9$5 3 for ITER *Nucl. Fusion* **58** 126010
[3] Pütterich T *et al* 2018 The ITER Baseline scenario investigated at ASDEX Upgrade *27th IAEA Int. Conf. on Fusion Energy* (*Gandhinagar, India, 2018*) (IAEA) p EX/8-4
[4] Schweinzer J *et al* (EUROfusion MST1 Team and ASDEX Upgrade Team) 2016 Development of the Q = 10 scenario for ITER on ASDEX Upgrade (AUG) *Nucl. Fusion* **56** 106007
[5] Garzotti L *et al* (JET Contributors) 2019 Scenario development for D-T operation at JET *Nucl. Fusion* **59** 076037
[6] Turco F, Luce T C, Solomon W, Jackson G, Navratil G A and Hanson J M 2018 The causes of the disruptive tearing instabilities of the ITER Baseline Scenario in DIII-D *Nucl. Fusion* **58** 106043
[7] Merle A, Sauter O and Yu Medvedev S 2017 Pedestal properties of H-modes with negative triangularity using the EPED-CH model *Plasma Phys. Control. Fusion* **59** 104001
[8] Fasoli A *et al* 2020 TCV heating and divertor upgrades *Nucl. Fusion* **60** 016019
[9] Sauter O *et al* 2021 ITER Baseline scenario investigations on TCV and comparison with AUG *28th IAEA Int. Conf. on Fusion Energy* (*Virtual Event, 2021*) (IAEA) p EX/4-887
[10] Pütterich T *et al* 2023 The stability of the H-mode entry in the ITER Baseline scenario investigated in AUG and TCV *29th IAEA Int. Conf. on Fusion Energy* (*London, UK, 2023*) (IAEA) p EX/7-2057
[11] Reimerdes H 2001 MHD stability limits in the TCV tokamak *EPFL Thesis* 2399 (available at: https://doi.org/10.5075/epfl-thesis-2399)
[12] Chapman I T *et al* (the ASDEX Upgrade, DIII-D, HL-2A, JT-60U, MAST, NSTX, TCV, Tore Supra Teams and JET-EFDA Contributors) 2010 Empirical scaling of sawtooth period for onset of neoclassical tearing modes *Nucl. Fusion* **50** 102001
[13] Pau A *et al* 2023 A modern framework to support disruption studies: the EUROfusion disruption database *29th IAEA Int. Conf. on Fusion Energy* (*London, UK, 2023*) (IAEA) p EX/4-1669
[14] Pau A, Cannas B, Fanni A, Sias G, Baruzzo M, Murari A, Pautasso G and Tsalas M (JET Contributors, ASDEX Upgrade Team and EUROfusion MST1 Team) 2017 A tool to support the construction of reliable disruption databases *Fusion Eng. Des.* **125** 139–53
[15] Van Mulders S *et al* 2023 Scenario optimization for the tokamak ramp-down phase in RAPTOR. Part A: analysis and model validation on ASDEX Upgrade *Plasma Phys. Control. Fusion* **66** 025006
[16] Teplukhina A A, Sauter O, Felici F, Merle A and Kim D (TCV Team, ASDEX Upgrade Team and EUROfusion MST1 Team) 2017 Simulation of profile evolution from ramp-up to ramp-down and optimization of tokamak plasma termination with the RAPTOR code *Plasma Phys. Control. Fusion* **59** 124004
[17] Contré C *et al* 2023 Rapid radial profiles simulation and scenario preparation on TCV using RAPTOR *49th EPS Conf. on Plasma Physics* (*Bordeaux, France, 2023*) p Fr_MCF48

[18] Sozzi C *et al* 2021 Termination of discharges in high performance scenarios in JET *28th IAEA Int. Conf. on Fusion Energy* (*Virtual Event, 2021*) (IAEA) p EX/3-77
[19] Labit B *et al* 2021 H-mode physics studies on TCV supported by the EUROfusion pedestal database *28th IAEA Int. Conf. on Fusion Energy* (*Virtual Event, 2021*) (IAEA) p EX/4-17
[20] Reimerdes H, Furno I, Hofmann F, Martynov A, Pochelon A and Sauter O 2006 Sawtooth behaviour in highly elongated TCV plasmas *Plasma Phys. Control. Fusion* **48** 1621
[21] Kong M (TCV Team and EUROfusion MST1 Team) 2019 Control of neoclassical tearing modes and integrated multi-actuator plasma control on TCV *Nucl. Fusion* **59** 076035